

The effect of the averaged structural and energetic features on the cohesive energy of nanocrystals

Ali Safaei

Received: 4 September 2009 / Accepted: 5 January 2010 / Published online: 3 February 2010
© Springer Science+Business Media B.V. 2010

Abstract The size dependency of the cohesive energy of nanocrystals is obtained in terms of their averaged structural and energetic properties, which are in direct proportion with their cohesive energies. The significance of the effect of the geometrical shape of nanoparticles on their thermal stability has been discussed. The model has been found to have good prediction for the case of Cu and Al nanoparticles, with sizes in the ranges of 1–22 nm and 2–22 nm, respectively. Defining a new parameter, named as the surface-to-volume energy-contribution ratio, the relative thermal stabilities of different nanoclusters and their different surface-crystalline faces are discussed and compared to the molecular dynamic (MD) simulation results of copper nanoclusters. Finally, based on the size dependency of the cohesive energy, a formula for the size-dependent diffusion coefficient has been presented which includes the structural and energetic effects. Using this formula, the faster-than-expected interdiffusion/alloying of Au_(core)–Ag_(shell) nanoparticles with the core–shell structure, the Au-core diameter of 20 nm and the Ag-shell thickness of 2.91 nm, has been discussed and the calculated diffusion coefficient has

been found to be consistent with its corresponding experimental value.

Keywords Nanocrystals · Clusters · Cohesive energy · Diffusion · Average coordination number · Modeling and simulation

Introduction

The diversity of the increasingly growing applications of nanocrystals in the rapidly changing world of nanotechnology is determined by their unique properties that are essentially different from those of bulk materials. These substantially different properties of nanoscaled matter from the bulk, which are structure-, shape-, and size-dependent, are heavily influenced by the heavily concentrated low-coordinated atoms at the surface of the nanocrystal. For example, the increased activity of supported nanocrystals can be attributed to the presence of a high portion of low-coordinated atoms in nanocrystals (Lopez et al. 2004). A change from bulk to molecular properties can occur when the coordination number of atoms decreases (DiCenzo et al. 1988), e.g., the bond nature evolution, resulting from the reduced coordination number of atoms, leads to a conductor–insulator transition (Rao et al. 2002). Also it has been stated that, due to the reduced coordination number of atoms at the surface of a metal, the preferred bond

Ali Safaei (✉)
Institute of Nano-Parthava, Mashhad, Iran
e-mail: ali.safaei@gmail.com

Ali Safaei
Zeus Engineering Technical Company, Mashhad, Iran

length within the plane of the metal surface is generally shorter than the bond length in the bulk (Needs and Mansfield 1989).

Therefore, in order to fully understand the way in which these properties changes with size, we need to gain knowledge about the volume-, and particularly, the surface-structure of nanocrystals. The average coordination number of nanocrystals is a parameter which can be used to averagely describe their structures. One of most important properties, dependent upon the surface-structure of nanocrystals, is their cohesive energy being an important coupling parameter for other physical–chemical properties, such as the Debye temperature, the diffusion activation energy, and the vacancy formation energy, etc (Yang and Li 2007). It has been recently proved that the cohesive energy of a nanocrystal can be well coupled with its average coordination number, which is only an averaged structural parameter (Attarian Shandiz et al. 2008; Mirjalili and Vahdati-Khaki 2008; Attarian Shandiz 2008). In this article, taking into account of the averaged effects of the first-nearest-neighbor (1NN), second-nearest-neighbor (2NN), and third-nearest-neighbor (3NN) interactions, we present a model for the cohesive energy of nanocrystals in terms of their energetic and structural features. Then, considering some simplifying assumptions, we develop a symmetrical proportion between the cohesive energy of elemental nanocrystals and their averaged 1-, 2-, and 3NN coordination numbers and energetic properties. Thereupon, with the use of the assumption that the energetic properties of the nanocrystal surface are the same as that of its volume and also by neglecting any likely size dependency of the atomic binding energy of nanocrystals, we obtain the recently developed, simple direct proportion between the cohesive energy and the 1NN-average coordination number of nanocrystals, presented in (Attarian Shandiz et al. 2008; Mirjalili and Vahdati-Khaki 2008; Attarian Shandiz 2008). This simple proportion, which has been based only upon the structural properties of nanocrystals, is the simplest approximation of the present model. Based on the proportionality between the melting point and cohesive energy (Yang and Li 2007), the present model for cohesive energy is applied to the melting point of elemental nanocrystals, and the effectiveness of its simplest form, i.e. its simplest approximation presented by Attarian Shandiz et al.

(2008), Mirjalili and Vahdati-Khaki (2008), and Attarian Shandiz (2008), is discussed for some elemental nanoparticles. It has been found that this approximation can only effectively predict the melting point variation of some restricted nanocrystals such as Cu and Al nanoparticles. It has also been seen that the molecular dynamic (MD) simulation results of the melting point of Cu nanoclusters (Delogu 2005; Wang et al. 2003) and the experimental data of Al nanoparticles (Lai et al. 1998; Sun and Simon 2007) are both higher than the predictions of some theoretical models, such as the liquid-drop model (LDM; Nanda et al. 2002), the model of the reference (Safaei et al. 2008), the homogenous melting model (HMM; Buffat and Borel 1976; Hanszen 1960; Pawlow 1909), and the model developed by Jiang et al. (2000, 2003). This discrepancy between the experiment and the theories is attributed to the significance of the effect of the structure and shape on the melting point of Cu and Al nanoparticles. Also with the use of the definition of a new parameter, named as the surface-to-volume energy-contribution ratio, the relative thermal stabilities of copper nanoclusters and different-crystalline faces on their surfaces are discussed, and the results are found to be consistent with the recently published findings of Daff et al. (2009). Also the higher prediction of the simple model represented in the references (Attarian Shandiz et al. 2008; Mirjalili and Vahdati-Khaki 2008; Attarian Shandiz 2008) for some elemental nanoparticles, such as Au, has been attributed to the neglected size dependency of the bonding energy of the surface atoms of these nanoparticles.

As a next step, we introduce a new lattice-type-sensitive formula for the size-dependent diffusion coefficient of atoms into nanocrystals, taking into account the effect of the volume (lattice) and surface structure of nanocrystals. This formula has been applied to the case of the mixing of $\text{Au}_{(\text{core})}\text{-Ag}_{(\text{shell})}$ nanoparticles to calculate the diffusion coefficient and time scale of their interdiffusion/alloying, which are found to be in good agreement with the corresponding experimental values reported by Hodak et al. (2000). It has finally been suggested that the faster-than-expected interdiffusion/alloying of $\text{Au}_{(\text{core})}\text{-Ag}_{(\text{shell})}$ nanoparticles occurs in the *solid phase*, and hence, it may be due to some structural effects, such as the depression of the average coordination number of nanoparticles, and is not

due to the surface melting of nanoparticles as has been stated by Hodak et al. (2000).

The model

The cohesive energy of nanocrystals

In Appendix 1, considering the effects of the first-nearest-neighbor (1NN) and the second-nearest-neighbor (2NN) atomic interactions, defining some structural averaged quantities, and neglecting any difference between the bond energies of volume atoms of nanocrystals and also between the bond energies of their surface atoms located at surface faces, surface edges and surface corners, we have found the below formula for the cohesive energy of nanocrystals (E_{cn}) as follows:

$$\frac{E_{cn}}{E_{cb}} = \frac{\bar{E}_V}{\bar{E}_{Vb}} \left(1 - \left(1 - \frac{\bar{E}_S}{\bar{E}_V} \right) \frac{n_S}{n_t} \right), \quad \Gamma = \frac{\bar{E}_S}{\bar{E}_V}. \quad (1)$$

Equation 1 is a general relation for the size-dependent cohesive energy of all types of crystalline nanosolids (nanocrystals), where Γ is a new parameter, named as the surface-to-volume energy-contribution ratio of the nanocrystal, which is defined here for the first time in this equation. \bar{E}_V and \bar{E}_S are, respectively, the average contributions of each volume and surface atom of the nanocrystal to its total cohesive energy, defined in Appendix 1. For all other definitions in this equation and in the coming equations, see Appendices 1–3. If we also consider the contribution of the third-nearest-neighbor (3NN) atoms to the cohesive energy of the nanocrystal, then we can obtain again Eq. 1 with $\Gamma = (\bar{Z}_S \varepsilon_S + \bar{Z}'_S \varepsilon'_S + \bar{Z}''_S \varepsilon''_S) / (\bar{Z}_V \varepsilon_V + \bar{Z}'_V \varepsilon'_V + \bar{Z}''_V \varepsilon''_V)$, where \bar{Z}'' and ε'' represent the corresponding parameters for the 3NN interactions, defined similarly as those of the 1- and 2NN atomic interactions in Appendix 1.

The cohesive energy and average coordination number of nanocrystals

Considering only the effect of the 1NN atoms, it has recently been found that the 1NN-based average coordination number of nanocrystals (\bar{Z}_n) is in direct proportion with their cohesive energy (E_{cn}), i.e. $E_{cn}/E_{cb} = \bar{Z}_n/\bar{Z}_b$ (Attarian Shandiz et al. 2008; Mirjalili and Vahdati-Khaki 2008; Attarian Shandiz 2008) where \bar{Z}_b is the average coordination number of the bulk crystal according to the 1NN definition.

Here, we show that this proportion is an approximation of the present model. Considering the effects of the 1NN and 2NN interactions, we have obtained the following relation in Appendix 2:

$$\frac{E_{cn}}{E_{cb}} = \frac{\varepsilon_V \bar{Z}_n}{\varepsilon_{Vb} \bar{Z}_b + \varepsilon'_{Vb} \bar{Z}'_b} \left(1 + \frac{\bar{Z}_S}{\bar{Z}_n} \left(\frac{\varepsilon_S}{\varepsilon_V} - 1 \right) \frac{n_S}{n_t} \right) + \frac{\varepsilon'_V \bar{Z}'_n}{\varepsilon_{Vb} \bar{Z}_b + \varepsilon'_{Vb} \bar{Z}'_b} \left(1 + \frac{\bar{Z}'_S}{\bar{Z}'_n} \left(\frac{\varepsilon'_S}{\varepsilon'_V} - 1 \right) \frac{n_S}{n_t} \right). \quad (2a)$$

Equation 2a shows a general relation between the cohesive energy and the average coordination number of nanocrystals, taking into account the effects of both of the averaged *structural* and *energetic* properties of their surface and volume. With the use of the assumptions $\varepsilon_S \approx \varepsilon_V$ and $\varepsilon'_S \approx \varepsilon'_V$, meaning that there is no significant difference between the bond energies of the surface and the volume atoms, we can write the following *first-order* approximation of Eq. 2a:

$$\frac{E_{cn}}{E_{cb}} = \frac{\varepsilon_V \bar{Z}_n + \varepsilon'_V \bar{Z}'_n}{\varepsilon_{Vb} \bar{Z}_b + \varepsilon'_{Vb} \bar{Z}'_b}, \quad \varepsilon_S \approx \varepsilon_V \quad \text{and} \quad \varepsilon'_S \approx \varepsilon'_V. \quad (2b)$$

Interestingly enough, there is a well-formulated symmetry in Eq. 2b. In addition to the effect of the averaged structural properties of the nanocrystal, Eq. 2b represents the effect of the energetic properties of volume atoms, ε_V and ε'_V , upon its cohesive energy. The ratios of $\varepsilon_V/\varepsilon_{Vb}$ and $\varepsilon'_V/\varepsilon'_{Vb}$ may have significant effects on the cohesive energy of nano-sized materials, due to the possible size dependency of the binding energy (Chacko et al. 2005). Taking into account the 3NN atoms, also leads to the similar equation as follows:

$$\frac{E_{cn}}{E_{cb}} = \frac{\varepsilon_V \bar{Z}_n + \varepsilon'_V \bar{Z}'_n + \varepsilon''_V \bar{Z}''_n}{\varepsilon_{Vb} \bar{Z}_b + \varepsilon'_{Vb} \bar{Z}'_b + \varepsilon''_{Vb} \bar{Z}''_b}. \quad (2c)$$

Now, neglecting the effect of the interactions between the 2NN and the 3NN atoms in Eq. 2c, i.e. $\varepsilon'_V/\varepsilon_V = \varepsilon''_V/\varepsilon_V \approx 0$ and $\varepsilon'_{Vb}/\varepsilon_{Vb} = \varepsilon''_{Vb}/\varepsilon_{Vb} \approx 0$, we can find the *second-order* approximation of Eq. 2a as follows:

$$\frac{T_{mn}}{T_{mb}} = \frac{E_{cn}}{E_{cb}} = \frac{\varepsilon_V \bar{Z}_n}{\varepsilon_{Vb} \bar{Z}_b}, \quad (2d)$$

where T_{mn} and T_{mb} are the melting points of nanocrystal and its bulk material, respectively. More importantly, as it can be seen from Eq. 2d, both of the averaged structural properties of nanocrystals and the energetic

properties of their volume atoms directly influence their cohesive energy and melting point. The importance of the effect of the volume energetic property (ε_V) in Eq. 2d can be well understood when we consider the proportionality of $E_{cn}/E_{cb} = E_{an}/E_{ab} = E_{vn}/E_{vb}$, proposed by Yang and Li (2007), where E_{an} and E_{vn} are the diffusion activation energy and the vacancy formation energy of nanocrystals, respectively, and E_{ab} and E_{vb} are the corresponding parameters for their bulk material. It is obvious that the diffusion activation and vacancy formation energies are dependent upon the *strength* of the atomic interactions (i.e. ε_V and ε'_V) as well as the *number* of neighbors of atoms (i.e. \bar{Z}_V , \bar{Z}_S , \bar{Z}'_V , \bar{Z}'_S , or averagely \bar{Z}_n and \bar{Z}'_n). Considering Eq. 2d and the above proportionality, it can be easily understood that the lower the binding energy and the average coordination number, the lower the diffusion activation and the vacancy formation energies.

The value of $\varepsilon_V/\varepsilon_{Vb}$ may have considerable effect for very small nanoparticles where the quantum-size effects may play an important role. However here, if we neglect any possible size dependency of ε_V and assume $\varepsilon_V/\varepsilon_{Vb} = 1$, we can obtain the *third-order* approximation of Eq. 2a as follows:

$$\frac{T_{mn}}{T_{mb}} = \frac{E_{cn}}{E_{cb}} = \frac{\bar{Z}_n}{\bar{Z}_b} \quad (2e)$$

Equation 2e is the simplest relation between the cohesive energy (or melting point) of nanocrystals and their 1NN-based average coordination number, which has recently been derived in the references (Attarian Shandiz et al. 2008; Mirjalili and Vahdati-Khaki 2008; Attarian Shandiz 2008). The assumptions of $\varepsilon_S/\varepsilon_V \approx 1$ and $\varepsilon_V/\varepsilon_{Vb} \approx 1$, which have been used to obtain Eq. 2e, may lead to some deviation in it, especially for very small nanocrystal sizes where the binding energies and bond lengths may be size-dependent and may need to consider the electronic structure effects (Chacko et al. 2005). In order to evaluate its effect in Eq. 2d, we need to know about the size dependency of ε_S and ε_V .

Another approximation of Eq. 2c can be obtained through consideration of the effects of the 1-, 2-, and 3NN atoms as well as assuming $\varepsilon_V \approx \varepsilon'_V \approx \varepsilon''_V$, $\varepsilon_{Vb} \approx \varepsilon'_{Vb} \approx \varepsilon''_{Vb}$, and $\varepsilon_V/\varepsilon_{Vb} = 1$. Therefore, we can write the other second-order approximation of Eq. 2a as:

$$\frac{T_{mn}}{T_{mb}} = \frac{E_{cn}}{E_{cb}} = \frac{\bar{Z}_n + \bar{Z}'_n + \bar{Z}''_n}{\bar{Z}_b + \bar{Z}'_b + \bar{Z}''_b} \quad (2f)$$

Equation 2f only shows the effect of the averaged structural properties of the nanocrystal on its cohesive energy and melting point in a symmetrical format.

The names of the above-mentioned approximations of Eq. 2a have only been chosen to indicate the numbers and the types of the required assumptions to obtain each approximation. For example, the third-order approximation, i.e. Eq. 2e, is obtained through using three types of assumptions: (i) the first assumption of equality between the surface and the volume energetic properties; (ii) the second assumption of neglecting the 2- and 3NN atomic interactions; and (iii) the third assumption of neglecting any possible size dependency of the bonding energy (ε_V), i.e. assuming that $\varepsilon_V/\varepsilon_{Vb} = 1$. These three types of assumptions are related to three different characteristics of each atom of a nanocrystal. The first assumption is related to the point that an atom located at the surface of the crystal is different from that located within its volume, and so gives different properties to the solid. The second assumption is related to the strength and the type of atomic bonds of a solid, which shows how long the range of interaction of an atom in a solid is. The third assumption is about the point that the atomic interactions may also be dependent upon the crystal's size, as well as being dependent upon the position of the atom in the solid (i.e. the surface or volume atoms) and/or the type of the solid (range of interactions).

According to the proportion given in the reference (Yang and Li 2007), other properties of nanocrystals such as their melting point, diffusion activation energy, vacancy formation energy, etc., similarly follow Eqs. 2a–d. In continuation, we first discuss about the accuracy of the prediction of Eq. 2e and the significance of the value of $\varepsilon_S/\varepsilon_V$ (in Eq. 2a), for some elemental nanoparticles, e.g., Au, Cu, and Al nanoparticles. After that we apply our model to study diffusion and rapid alloying at the nanoscale.

Results and discussion

The significance of energetic effects on melting point of nanoparticles

As it has been discussed, through neglecting any likely size dependency of the atomic bonding energy

in Eq. 2d, we can obtain Eq. 2e which has recently been introduced in the references (Attarian Shandiz et al. 2008; Mirjalili and Vahdati-Khaki 2008; Attarian Shandiz 2008). Equation 2e simply demonstrates only the effect of the nanocrystal's geometry on its cohesive energy and, consequently, on its melting point (or its other physical properties). Here, we use Eq. 2e for the prediction of melting point of nanoparticles (T_{mp}). The size-dependent geometrical characteristics of nanoclusters and especially their 1NN-average coordination number (denoted by \bar{Z}_{clu}) have been presented by Montejano-Carrizales et al. (1997) as a function of the cluster order (v —the number of crusts forming the cluster). Assuming that relatively large nanoparticles (with diameters larger than 6 nm) can be considered as spheres (Wautelet 1998) and approximately equivalent to the nanoclusters described by Montejano-Carrizales et al. (1997), one can use their obtained 1NN-average coordination number (\bar{Z}_{clu}) as an approximation for the nanoparticles average coordination number in Eq. 2e. Therefore, Mirjalili and Vahdati-Khaki (2008) have recently used Eq. 2e with the size-dependent functions of \bar{Z}_{clu} , reported in the reference (Montejano-Carrizales et al. 1997), to predict the melting point variations of some simple-cubic (SC), body-centered cubic (BCC), and face-centered cubic (FCC) nanoparticles. If we plot Eq. 2e by assuming $\bar{Z}_n \approx \bar{Z}_{clu}$, i.e. $T_{mp}/T_{mb} \approx \bar{Z}_{clu}/\bar{Z}_b$, and using \bar{Z}_{clu} functions of each structure from the reference (Montejano-Carrizales et al. 1997), then we can find that the predictions of Eq. 2e is generally higher than the experimental data of the melting points of Au, Pb, In, Sn, and Bi nanoparticles, especially for small nanoparticles. This can also be understood if we see the graphs of Au, Pb, In, Sn, and Bi nanoparticles, plotted by Mirjalili and Vahdati-Khaki (2008). For brevity, we do not plot these graphs here, which are found in Mirjalili and Vahdati-Khaki (2008). This result motivates us to ask, for which elements and shapes, Eq. 2e (using $\bar{Z}_n \approx \bar{Z}_{clu}$) is applicable. The reason for this discrepancy between the prediction of Eq. 2e and the experimental data for these nanoparticles is not obvious, but there are some likely tentative explanations. It is possible that the shapes of Au, Pb, In, Sn, and Bi nanoparticles at their corresponding experimental conditions could not be completely considered as the nanoclusters described by Montejano-Carrizales et al. (1997), and therefore $\bar{Z}_n \approx \bar{Z}_{clu}$ may

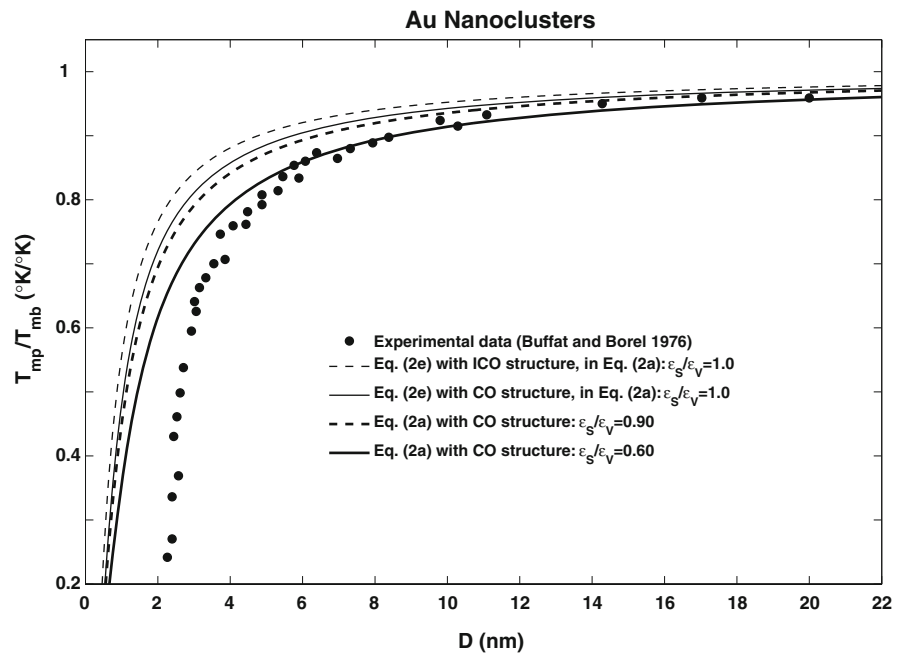
not be actually accurate. The other possible explanation is that, for these particles ε_V in Eq. 2d may be size dependent, especially for small particles, and therefore assuming $\varepsilon_V/\varepsilon_{Vb} \approx 1$ in Eq. 2e may cause this deviation from the experimental data. Also it is worthy to note that the size dependency of the ratio of $\varepsilon_S/\varepsilon_V$ in Eq. 2a may have significant effect on the cohesive energy of nanocrystals; therefore, the assumption of $\varepsilon_S/\varepsilon_V \approx 1$ in Eq. 2a, may be another possible reason for the deviation of Eq. 2e from the experimental data. We shall discuss about the case of Au nanoparticles.

Au nanoparticles

Here, we discuss about the case of Au nanoparticles. Solliard and Flueli (1985) investigated the effect of the surface stress and size on the lattice parameter of small gold particles. They found that the surface of the gold particles was in a state of tension, and therefore interatomic distances at the surface was greater than the distances characterizing an *infinite* (111) plane of gold at equilibrium; i.e. a 5% dilatation had occurred in the surface faces of the icosahedron gold clusters (Solliard and Flueli 1985). This means that the bond length of the surface atoms of small gold particles is longer than that of the surface of the *bulk* gold. It has also been found that the lattice constant of gold particles decreases with decreasing their size (Solliard and Flueli 1985); meaning that, in general, the *average* interatomic spacing in the gold particles decreases with decreasing their size (Solliard and Flueli 1985). This finding also means that on average the bond length of the gold particles is shorter than the average bond length of the bulk gold. These findings implicitly mean that the bond length of the surface atoms of gold nanoparticles is longer than that of their volume atoms; meaning that the surface bonds are weaker than the volume bonds of the gold particles; i.e. $\varepsilon_S/\varepsilon_V < 1$.

We have plotted Eqs. 2a and 2e for gold nanoparticles in Fig. 1, compared with the experimental data of the reference (Buffat and Borel 1976). The lattice structure of gold is FCC, and hence in order to plot Eq. 2e, we assumed that FCC nanoparticles are approximately equivalent to the cubo-octahedral (CO) and/or the icosahedral (ICO) clusters described by Montejano-Carrizales et al. (1997). The average

Fig. 1 The dependence of the melting point of Au nanoparticles on their size. Equations 2a and 2e are compared to the experimental data (Buffat and Borel 1976). For bulk Au: $T_{mb} = 1337.3$ K (Lide 2005) and its atomic radius is $r = 0.1594$ nm deduced from its atomic volume (Nanda et al. 2002)



coordination number of the CO (\bar{Z}_{clu}^{CO}) and the ICO (\bar{Z}_{clu}^{ICO}) clusters have been calculated as follows (Montejano-Carrizales et al. 1997): $\bar{Z}_{clu}^{CO} = 24v(5v^2 + 3v + 1)/(10v^3 + 15v^2 + 11v + 3)$ and $\bar{Z}_{clu}^{ICO} = 6v(20v^2 + 15v + 7)/(10v^3 + 15v^2 + 11v + 3)$. Therefore, the melting point of FCC nanoparticles can be obtained from Eq. 2a and 2e with the use of $\bar{Z}_n \approx \bar{Z}_{clu}^{CO}$ and/or $\bar{Z}_n \approx \bar{Z}_{clu}^{ICO}$, and $\bar{Z}_b = 12$. Using these values and $v = (D/d - 1)/2$, we have plotted Eqs. 2a and 2e in terms of the nanoparticles diameter (D).

As shown in Fig. 1, the use of ICO structure gives higher prediction than using CO structure; therefore, we now assume that Au nanoparticles, investigated by Buffat and Borel (1976), are nearly CO nanoclusters. It can be seen from the figure that the prediction of Eq. 2e is higher than the melting point experimental data of gold nanoparticles. However, plotting Eq. 2a with the value of $\varepsilon_S/\varepsilon_V = 0.9$, and without considering the 2NN interactions, gives good consistency with the melting point experimental data of gold nanoparticles having diameters approximately larger than 10 nm. However, for smaller particles a larger reduction of the ratio of $\varepsilon_S/\varepsilon_V$ is expected; and the value of $\varepsilon_S/\varepsilon_V = 0.6$ is nearly suitable for this range of sizes. Our finding, that $\varepsilon_S/\varepsilon_V < 1$, is qualitatively consistent with the finding of Solliard and Flueli (1985) that the bond length of the surface atoms is longer than the volume atoms; however,

Eq. 2a requires a larger decrease of the ratio of $\varepsilon_S/\varepsilon_V$ with decreasing gold nanoparticles size. Quantitatively, we can refer to the amount of the dilation (5%) within the surface of Au (Solliard and Flueli 1985). Considering this value, one can conclude that $a_S^{after}/a_S^{before} \approx 1.05$ where a_S^{after} and a_S^{before} are the averaged interatomic distances within the surface of Au nanoparticles after and before their surface dilation, respectively. Assuming that the bond energy is in inverse proportion to the interatomic distance, we can find $\varepsilon_S^{after}/\varepsilon_S^{before} \approx 0.95$, where ε_S^{after} and ε_S^{before} are the average bond energies of surface atoms after and before the dilation within the surface faces, respectively. Here, if we assume that the bond energy of surface atoms before dilation is approximately equal to that of the volume atoms, then we can have: $\varepsilon_S^{after}/\varepsilon_V \approx 0.95$, which is fairly in agreement with the value of $\varepsilon_S/\varepsilon_V \approx 0.90$, used by us, for Au nanoparticles larger than 10 nm; however, for smaller particles, we expect a larger depression of the ratio of $\varepsilon_S/\varepsilon_V$.

For other elements, such as Pb, In, Sn, and Bi, the higher prediction of Eq. 2e compared with the experimental data (see Mirjalili and Vahdati-Khaki 2008), also indicates that the bond energy of the surface atoms of these nanoparticles may be smaller than that of the volume atoms, i.e. $\varepsilon_S/\varepsilon_V < 1$, and also may decrease with decreasing their size. However, this is in direct contradiction to the results

previously obtained for the bond length of surface atoms. In general, it has been found that, owing to the lower coordination number of atoms, the preferred bond length within the plane of a metal surface is shorter than the bond length in the bulk (Mansfield and Needs 1991; Needs and Mansfield 1989; Salomons et al. 1988). All of these investigations are for a surface of a bulk crystal and the bond length has been compared with that of the volume of the bulk crystal. Therefore, the size dependency of the ratio of ϵ_S/ϵ_V for nanocrystals of these elements is still unknown. Hence, it requires further investigation to clarify this point that, for which elements, the surface atomic bonds are weaker and/or stronger than the volume atomic bonds in nanoscale.

Now, we do not have any appropriate size-dependent function for ϵ_S/ϵ_V to evaluate its effect on melting point of nanoparticles; we only represent two cases of nanoparticles (Al and Cu with FCC lattice) whose melting point variations are fully consistent with the consideration of only geometrical

effects, i.e. with the prediction of Eq. 2e when we use $\bar{Z}_n \approx \bar{Z}_{clu}$.

The significance of geometrical effects on melting point of nanoparticles

Cu nanoparticles

As shown in Fig. 2, the prediction of the model of Jiang et al. (2000, 2003), LDM (Nanda et al. 2002), and our previous model (Safaei et al. 2008) are all lower than the MDs results of the melting point of Cu nanoparticles (Delogu 2005; Wang et al. 2003). Now the reason for this deviation is not clear to us. However, using the average coordination number of the CO and ICO clusters, it is found that the prediction of Eq. 2e is fully consistent with these MD results. As shown in Fig. 2, using $\bar{Z}_n \approx \bar{Z}_{clu}^{CO}$ gives the better consistency with the MD results of the references (Delogu 2005; Wang et al. 2003) than using $\bar{Z}_n \approx \bar{Z}_{clu}^{ICO}$. This implies that the Cu nanoparticles investigated by Delogu (2005) and also by

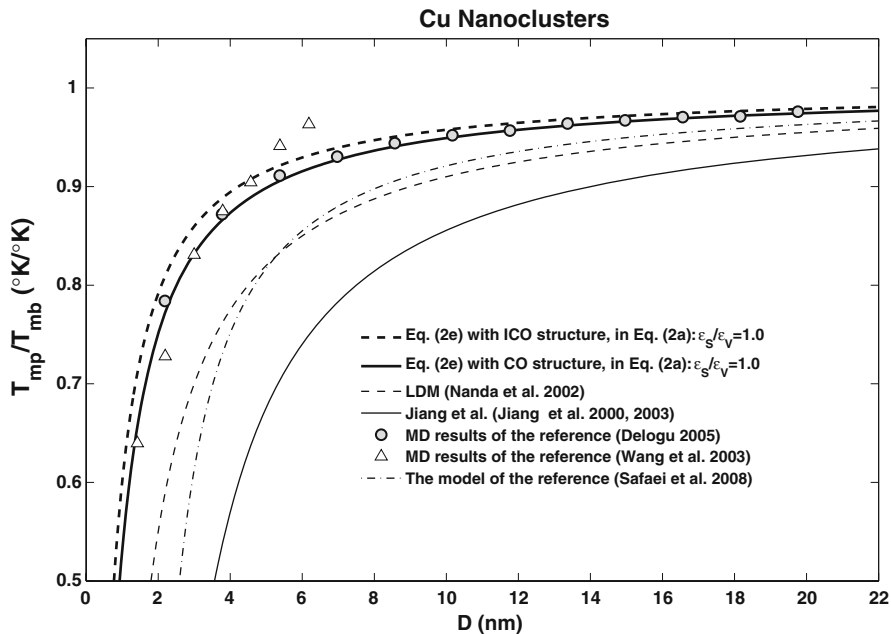


Fig. 2 The size-dependence of the melting point of Cu nanoclusters: Eq. 2e is compared to the LDM (Nanda et al. 2002); Jiang et al. (2000, 2003) and the model of (Safaei et al. 2008) as well as the MD results (Delogu 2005; Wang et al. 2003). The melting point data of the reference (Delogu 2005; denoted by circles) has been divided by the value of $T_{mb}^{simu.} = 1250$ K which has been obtained by the bulk simulation of Cu

crystals by Delogu (2005). Also the data of the reference (Wang et al. 2003; shown by triangles) has been divided by $T_{mb}^{extra.} = 1360$ K which has been obtained through extrapolating the obtained data for the bulk Cu crystal by Wang et al. (2003). The atomic radius of Cu is $r = 0.1413$ nm deduced from its atomic volume (Nanda et al. 2002)

Wang et al. (2003) may have had the CO structure rather than the ICO structure. This can be verified from the way in which Delogu built the Cu nanoparticles. Considering one of the atoms in the central region of the Cu bulk crystal as the center of a sphere of diameter D , Delogu (2005) individuated approximately spherical crystalline portions of the bulk Cu with FCC structure. Therefore, the nanosized crystalline particles, investigated by Delogu (2005), consisted of the atoms positioned within the sphere of diameter D with the FCC arrangement. As we know, the geometry obtained by the FCC arrangement of atoms in a sphere, with an atom located at the center of the sphere, is a CO cluster having the *non-compact* crystalline faces as well as the closest-packed faces [(111) faces]. For more information about the ICO and CO clusters, see Montejano-Carrizales et al. (1997) to find that the ICO clusters have only triangular faces (*closest-packed* faces) on their surfaces and the CO clusters have both the closest-packed and non-closest-packed faces on their surfaces. Therefore, the Cu nanoparticles, built and

investigated by Delogu (2005), had the CO geometry, which is fully consistent with the better prediction of Eq. 2e using $\bar{Z}_n \approx \bar{Z}_{\text{clu}}^{\text{CO}}$ rather than using $\bar{Z}_n \approx \bar{Z}_{\text{clu}}^{\text{ICO}}$. This clearly implies the importance of the effects of the geometrical arrangement of atoms in nanoclusters, and especially at their *surface*, upon their melting point and thermal stability.

Al nanoparticles

Shown in Fig. 3 are the graphs of Jiang et al. model (2000, 2003), LDM (Nanda et al. 2002), HMM (Buffat and Borel 1976; Hanszen 1960; Pawlow 1909), and our previous model (Safaei et al. 2008) as well as the experimental data obtained by Lai et al. (1998) and by Sun and Simon (2007). As it can be seen, all the theoretical models underestimate both sets of the experimental data. Now, we conjecture the possible reasons of this contradiction between the experiment and the theory. The first reason coming to mind is that the investigated Al nanoparticles were coated by an oxide layer. However, this idea can be

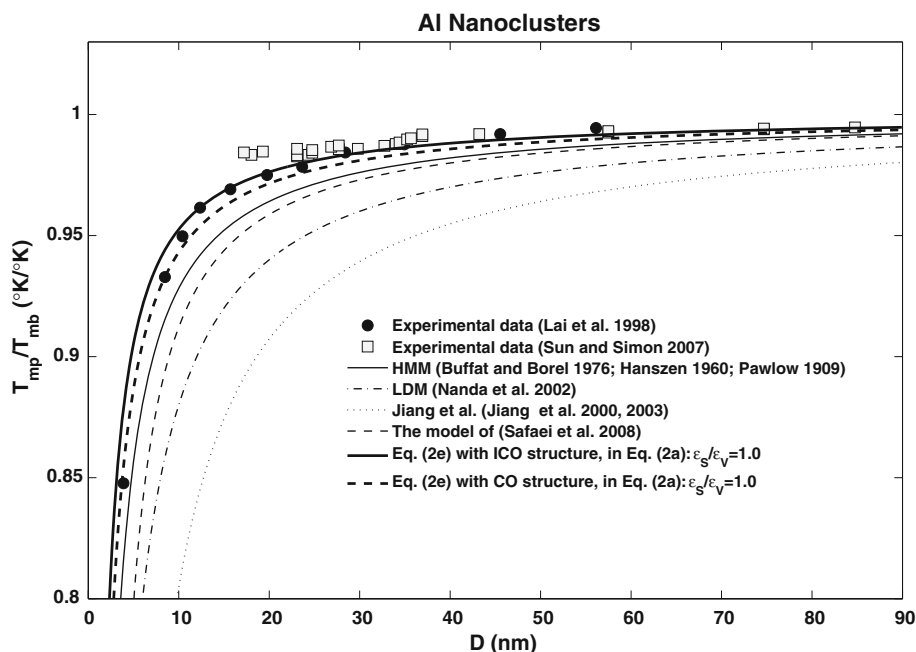


Fig. 3 The size-dependence of the melting point of Al nanoclusters: Eq. 2e compared to the LDM (Nanda et al. 2002), the model of (Safaei et al. 2008), HMM (Buffat and Borel 1976; Hanszen 1960; Pawlow 1909) and Jiang et al. (2000, 2003). The experimental data are from the references

(Lai et al. 1998; Sun and Simon 2007). For Bulk Al: $T_{\text{mb}} = 933.47$ K (Lide 2005) and its atomic radius is $r = 0.1583$ nm deduced from its atomic volume (Nanda et al. 2002)

rejected by looking through the experiments performed by Lai et al. (1998) and by Sun and Simon (2007). Lai et al. (1998) investigated the discontinuous Al films, including the collection of individual Al nanoparticles, deposited on the Si_3N_4 membrane. They have reported that no oxide layer was formed on the surface of the Al nanoparticles.

Sun and Simon (2007) examined the melting behavior of aluminum nanoparticles having an oxide passivation layer. They reported that the effect of the oxide layer on the particles is to apply a compressive force to the aluminum core, thus increasing the observed melting point. However, they corrected their measured melting points taking into account for the effects of the oxide layer. Here, in Fig. 3, we have plotted their corrected melting point data which are close to the data obtained by Lai et al. (1998) and, hence, one can conclude that the oxide shell effects on the melting point were accurately eliminated by Sun and Simon (2007). Therefore, we conclude that the discrepancy between the experimental results and the theoretical predictions may be due to other reasons such as the geometrical effects as the case of Cu nanoparticles and/or some other things.

Here, we provide a likely explanation for the deviation between the experiment and the theoretical models for the melting point of Al nanoparticles. It is possible that the geometry of Al nanoparticles investigated by Lai et al. (1998) and by Sun and Simon (2007) could not be considered as what we assumed, for plotting the above-mentioned theoretical models, to be spherical particles with no significant numbers of the surface edges and surface corners. If we plot Eq. 2e, using $\bar{Z}_n \approx \bar{Z}_{\text{clu}}^{\text{ICO}}$ and $\bar{Z}_n \approx \bar{Z}_{\text{clu}}^{\text{CO}}$, we can find that the melting point experimental data can be well fitted by $\bar{Z}_n \approx \bar{Z}_{\text{clu}}^{\text{ICO}}$ much better than by $\bar{Z}_n \approx \bar{Z}_{\text{clu}}^{\text{CO}}$ (see Fig. 3). This means that the geometrical shape of the Al nanoparticles in their experimental conditions may have been the ICO clusters rather than the CO clusters and also not that geometry (a spherical particle with no surface edges and surface corners) assumed for plotting the LDM (Nanda et al. 2002), the model of Jiang et al. (2000, 2003), and our previous model (Safaei et al. 2008). Therefore, we think, the main reason for the deviation between the theory and the experiments is the difference between the theoretically assumed geometrical shape of the Al nanoparticles (i.e. spheres) and their actual shape in the experimental conditions.

The relative thermal stabilities of nanoclusters and of their surface faces

Now, we discuss about the usefulness of our defined new factor, named as the surface-to-volume energy-contribution ratio (Γ), while comparing the thermal stability of different shapes of clusters. The higher thermal stability of the ICO clusters compared to the CO clusters (shown in Figs. 1, 2, 3) can be predicted by comparing the Γ factors of these two structures from Eq. 22 or Eq. 1. For FCC nanoparticles, using Eq. 22 with the only 1NN interactions, i.e. $\Gamma \cong \bar{Z}_S \varepsilon_S / \bar{Z}_V \varepsilon_V$, assuming $\bar{Z}_V = 12$ and $\varepsilon_S = \varepsilon_V$, and using the surface-average coordination numbers of the ICO and CO clusters proposed in the reference (Montejano-Carrizales et al. 1997) for \bar{Z}_S , we can find: $\Gamma^{\text{ICO}} = 30v^2 / (12(5v^2 + 1)) > \Gamma^{\text{CO}} = 24v^2 / (12(5v^2 + 1))$. Therefore, if there is no other stabilizer forces, then the ICO cluster is more stable than the CO cluster. This higher thermal stability of the ICO cluster compared with the CO cluster of the same number of atoms can be attributed to the type of the surface-crystalline faces. The ICO cluster has only the closest-packed faces on its surface, while the CO cluster has also noncompact crystalline faces as well as the closest-packed faces (Montejano-Carrizales et al. 1997). As shown in Fig. 3, the experimentally investigated Al nanoparticles (Lai et al. 1998; Sun and Simon 2007) may have had the ICO geometry, while the Cu nanoparticles investigated by MD methods (Delogu 2005; Wang et al. 2003) were close to the CO geometry, because they were built by intentionally arranging, and not by self-derived arranging, the atoms in FCC sites within a sphere of diameter D (Delogu 2005). Hence, much more importantly, it is expected that the self-assembled FCC nanoparticles have approximately the ICO geometry rather than the CO. This is in agreement with the findings of Daff et al. (2009), that the most stable shapes of copper nanoclusters are those having a combination of (111) and (100) surface faces with a greater proportion of (111) faces at their surfaces.

Besides being a useful factor to compare the relative thermal stabilities of different nanocrystals, the new factor Γ has another important usefulness in comparing the relative thermal stabilities of different crystalline faces located at the nanocrystal surface. Taking into account the effects of the 1-, 2-, and 3NN atomic interactions, we have calculated the values of

Γ for the (111), (100), (110), and (210) faces of a FCC lattice structure in Appendix 3. Considering Eq. 31, we can conclude that $\Gamma_{(111)} > \Gamma_{(100)}$, $\Gamma_{(111)} > \Gamma_{(110)}$ and $\Gamma_{(110)} > \Gamma_{(210)}$. Also with the use of Eq. 31, we have $\Gamma_{(100)} - \Gamma_{(110)} \cong 2(\varepsilon - \varepsilon')/(12\varepsilon + 22\varepsilon')$. Since the strength of the 1NN interactions is more than that of the 2NN interactions, i.e. $\varepsilon > \varepsilon'$, we can conclude that $\Gamma_{(100)} - \Gamma_{(110)} > 0$; and, finally, we have $\Gamma_{(111)} > \Gamma_{(100)} > \Gamma_{(110)} > \Gamma_{(210)}$.

Due to its definition (in Eq. 22), Γ is a factor representing the average contribution of each surface-crystalline face to the cohesive energy of the nanocrystal. Hence, this factor is a criterion for the relative thermal stability of a surface-crystalline face of a nanocrystal. In other words, the more the value of Γ for a surface face, the more the thermal stability of that face. Therefore, we can conclude that the thermal stabilities of the low index surface faces of a FCC nanocrystal is in the order of (111) > (100) > (110) > (210). More interestingly, this is exactly the same conclusion made by Daff et al. (2009) in their newly published article. They have recently conducted a theoretical research on the effect of atomic structure and coordination number on the stabilities and melting behavior of copper surfaces and nanoclusters (Daff et al. 2009). The two important conclusion, they have made thorough their MD simulations, are: (I) the surface melting was observed to occur below the bulk melting point, at *increasingly* lower temperatures from the (111), (100), and (110) faces down to the (210) face, confirming their order of decreasing stability; and (II) the ordering of the stabilities of these surface faces does not vary with temperature, and their relative values remain the same. These two conclusions are well consistent with our findings that: $\Gamma_{(111)} > \Gamma_{(100)} > \Gamma_{(110)} > \Gamma_{(210)}$ (we assume that this order of Γ -factors for these faces is temperature independent).

The investigation of Daff et al. (2009) has also yielded the result that melting begins at the location of low-coordinated atoms in the surface, such as the atoms located at the surface steps, and especially those steps with lower coordination numbers. This conclusion can also be achieved through calculating Γ for different surface-crystalline edges and comparing them to each other.

Here, we discuss about the significance of the effect of another structural feature upon the stability

of crystals, which is the atomic packing arrangement and is averagely defined here for the first time as

$$\bar{P}_S = \bar{P}_f \cdot x_f^{\text{area}} + \bar{P}_e \cdot x_e^{\text{area}} + \bar{P}_c \cdot x_c^{\text{area}}, \quad (3)$$

where \bar{P}_S is the average packing factor of the surface of the nanocrystal, \bar{P}_f is the average face-packing factor of the surface faces of the nanocrystal, \bar{P}_e is the average-edge-packing fraction of the edges of the nanocrystal surface, and \bar{P}_c is the corner-packing fraction ($\bar{P}_c = 1$). These packing fractions are defined as the ratios of the filled areas of the surface faces, surface edges, and surface corners by atoms to the total area of the nanocrystal surface corresponding to these surface sites, i.e. $\bar{P}_f = n_f A_a / A_f$, $\bar{P}_e = n_e A_a / ((L_e/d) \cdot A_a)$ and $\bar{P}_c = (n_c A_a) / (n_c A_a) = 1.0$, where $A_a = \pi d^2 / 4$ is the cross-sectional area of a surface atom with the nanocrystal surface. n_f , n_e and n_c are respectively the total number of atoms located at all the surface-crystalline faces, surface-edges and surface-corners. A_f , $(L_e/d) \cdot A_a$, and $n_c A_a$ are the total areas of the surface faces, surface edges, and surface corners, respectively, which are the portions of the total surface area of the crystal (A_S) which can be *potentially* occupied by the face-, edge-, and corner-atoms, respectively. The area fraction (x^{area}) of each type of surface sites (faces, edges, or corners) is defined as the ratio of the area amount of the crystal surface associated with that surface site, being occupied or unoccupied by atoms, to the total area of the crystal surface (A_S). Hence, $x_f^{\text{area}} = A_f / A_S$ is the area fraction of the surface faces, $x_e^{\text{area}} = (L_e/d) \cdot A_a / A_S$ is the area fraction of the surface edges, and $x_c^{\text{area}} = (n_c A_a) / A_S$ is the area fraction of the surface corners (note that $x_f^{\text{area}} + x_e^{\text{area}} + x_c^{\text{area}} = 1$). Considering these definitions, we can find the following relations:

$$\begin{aligned} \frac{n_f}{n_S} &= \frac{\bar{P}_f}{\bar{P}_S} \cdot x_f^{\text{area}}, & \frac{n_e}{n_S} &= \frac{\bar{P}_e}{\bar{P}_S} \cdot x_e^{\text{area}}, \\ \text{and } \frac{n_c}{n_S} &= \frac{\bar{P}_c}{\bar{P}_S} \cdot x_c^{\text{area}}. \end{aligned} \quad (4)$$

Now merging Eq. 4 with Eq. 19, we can rewrite the 1NN, surface average coordination number as:

$$\bar{Z}_S = \frac{\bar{P}_f \cdot x_f^{\text{area}} \bar{Z}_f + \bar{P}_e \cdot x_e^{\text{area}} \bar{Z}_e + \bar{P}_c \cdot x_c^{\text{area}} \bar{Z}_c}{\bar{P}_S} \quad (5)$$

Interestingly enough, Eqs. 3 and 5 present a well-formulated, new, size-dependent definition of the surface average-packing factor and surface average

coordination number of the nanocrystal, including the effects of the average atomic arrangement of the surface faces, surface edges, and surface corners. For the bulk crystal ($x_e^{\text{area}} \rightarrow 0, x_c^{\text{area}} \rightarrow 0$): $x_f^{\text{area}} \rightarrow 1$, and therefore $\bar{P}_{Sb} = \bar{P}_{fb}$, and $\bar{Z}_{Sb} = \bar{Z}_{fb}$, implying that the only important factor for the bulk crystal is its averaged surface face atomic arrangement.

Equation 5 can be written in the following well-arranged form:

$$\begin{aligned} \bar{P}_S \bar{Z}_S &= (\bar{P}_f \bar{Z}_f) \cdot x_f^{\text{area}} + (\bar{P}_e \bar{Z}_e) \cdot x_e^{\text{area}} + (\bar{P}_c \bar{Z}_c) \cdot x_c^{\text{area}} \\ &= \sum_{j=f, e, c} (\bar{P}_j \bar{Z}_j) \cdot x_j^{\text{area}} \end{aligned} \tag{6}$$

Equations 5 and 6 are also true for 2- and 3NN coordination numbers. In Eq. 6, $\bar{P}_S \bar{Z}_S$ is a well-formulated quantity that is composed of three components: the face component ($\bar{P}_f \bar{Z}_f$), the edge component ($\bar{P}_e \bar{Z}_e$), and the corner component ($\bar{P}_c \bar{Z}_c$). The crystal surfaces with highly packed atomic arrangement, i.e. having the larger values of \bar{P}_S and \bar{Z}_S , are more stable than the others. Therefore, the combined effects of both of the structural features of the surface, i.e. the atomic packing factors and coordination numbers, are interestingly represented in parameter $\bar{P}_S \bar{Z}_S$. In addition to these structural features, the energetic features of the surface of a crystal are also of great importance while determining its thermal stability. Hence, we define a new parameter, named as the averaged surface energy density (SED) of a crystal as follows:

$$\langle \text{SED} \rangle = \bar{P}_S \bar{Z}_S \bar{\varepsilon}_S \tag{7}$$

where $\bar{\varepsilon}_S$ is the average bonding energy of the crystal surface. It can be inferred from Eq. 7 that the physical dimension of average SED is $\frac{\text{atom}}{\text{unit area}} \times \frac{\text{bonds}}{\text{atom}} \times \frac{\text{energy}}{\text{bond}}$ (i.e. energy-per-unit area). Therefore, it can be defined as

$$\begin{aligned} \langle \text{SED} \rangle &= \frac{\int \int_{A_S} ED_{(x,y,z)} \cdot dA}{A_S}, \\ ED_{(x,y,z)} &= \frac{dE_{(x,y,z)}}{dA} = \frac{\partial^2 E_{(x,y,z)}}{\partial x \partial y}, \end{aligned} \tag{8}$$

where $ED_{(x,y,z)}$ and $E_{(x,y,z)}$ are the local energy density and the local cohesive energy at each point (i.e. each atom) (x, y, z) of the crystal, respectively.

More importantly, the averaged SED has the combination of the effects of *the averaged structural and energetic features* of the surface and is also a *temperature-dependent* quantity. Therefore, we

conjecture that it can be used as a criterion for the thermal stability of a nanocrystals surface, and particularly, that its abrupt change near the melting point can be used as a signature for the onset temperature of surface melting. Hence, an important subject about the stability of nanoclusters, that can be an interesting topic for further investigation and particularly for computer simulation studies, is the question of finding the numbers of and/or the area fractions of each type of surface faces and surface edges to precisely calculate the values of \bar{Z}_S (Eq. 5) and \bar{P}_S (Eq. 3) and then accurately calculate $\bar{P}_S \bar{Z}_S$ and/or SED. Similar to Eq. 7, an averaged quantity can also be defined for a nanocrystal which can be used as an indicator of its thermal stability and the beginning of its melting.

We now discuss about the implications of the size-dependent cohesive energy to the diffusion coefficient of atoms in the nanocrystals, especially to the size-dependent alloying of core-shell bimetallic nanoparticles.

Size-dependent diffusivity

We assume that a well-known Arrhenius dependence for diffusion coefficient, $DC_{(X,T)}$, is also applicable for nanocrystals as

$$DC_{(X,T)} = DC_{0(X)} \exp\left(\frac{-E_{an}(X)}{RT}\right), \tag{9}$$

where X is the reciprocal size of the nanocrystal, $DC_{0(X)}$ is the pre-exponential constant (temperature-independent factor) for nanocrystals, R is the ideal gas constant, T is the absolute temperature, and E_{an} is the diffusion activation energy of the nanocrystal. Considering the proportionality of $E_{an}/E_{ab} = T_{mn}/T_{mb}$ (Yang and Li 2007), and assuming that the diffusion coefficient at *the melting point of a nanocrystal is size independent*, i.e. $DC_{(X,T_{mn})} = DC_{b(T_{mb})}$ and *also that the diffusion activation energy is temperature independent* (Dick et al. 2002), we can conclude from Eq. 9: $DC_{0(X)} = DC_{0b}$, where DC_{0b} is the pre-exponential constant of Eq. 9 for the bulk crystal. Therefore, hereafter for simplicity, we use the notation of DC_0 as the abbreviation of $DC_{0(X)}$ and DC_{0b} . Thus, we can write:

$$DC_{(X,T)} = DC_0 \exp\left(\frac{-E_{ab}}{RT} \cdot \frac{T_{mn}}{T_{mb}}\right), \tag{10}$$

where E_{ab} is the diffusion activation energy for the bulk crystal. If we substitute our previously obtained formula for the melting point of nanocrystals (Safaei et al. 2007, 2008) in Eq. 10, then we can find a lattice-type-sensitive formula for the size and temperature dependency of the diffusion coefficient of nanocrystals. Equation 10 can also be rewritten in the following form:

$$\frac{DC_{(X,T)}}{DC_0} = \left(\frac{DC_{b(T)}}{DC_0} \right)^{\frac{T_{mb}}{T_{mp}}} \quad (11)$$

Using Eq. 2d, the above equation can be written in terms of the average coordination number of the nanocrystal and its binding energy as follows:

$$\frac{DC_{(X,T)}}{DC_0} = \left(\frac{DC_{b(T)}}{DC_0} \right)^{\frac{\varepsilon_V \bar{Z}_n}{\varepsilon_{Vb} \bar{Z}_b}} \quad (12)$$

Equation 12 clearly shows the effects of the averaged *energetic and structural feature* on the diffusivity of atoms in nanocrystals. Assuming that $\varepsilon_V = \varepsilon_{Vb}$, we can simply write:

$$\frac{DC_{(X,T)}}{DC_0} = \left(\frac{DC_{b(T)}}{DC_0} \right)^{\frac{\bar{Z}_n}{\bar{Z}_b}} \quad (13)$$

In order to obtain Eq. 10 and so Eq. 13, it has been assumed that the diffusion coefficient at melting point is size independent. Considering this assumption, we can find from Eq. 13 that $\bar{Z}_n(X, T_{mn}(X)) = \bar{Z}_b(T_{mb})$. Here, this importantly implies that the average coordination number of nanocrystals at their melting point is a size-independent quantity. It can be conjectured that this conclusion may also be true for a droplet of a liquid, and that its diffusion coefficient may be independent from its size.

Now, we discuss about the alloy formation in the nanoscale. Hodak et al. (2000) synthesized bimetallic gold–silver nanoparticles with a core–shell structure by irradiation chemistry. They investigated the laser-induced interdiffusion in Au–Ag core–shell nanoparticles and found that the transformation from the abrupt metal–metal junction into a homogeneous alloyed nanoparticle reached completion after many laser pulses (Hodak et al. 2000). They reported that for the Au_(core)–Ag_(shell) nanoparticles with the Au-core diameter of 20 nm and Ag-shell thickness of 2.91 nm (with the concentrations ratio of [Au]:[Ag] = 1:0.5), significant alloying started when the absorbed energies were

about 0.35 mJ/pulse, and therefore, the temperature of the sample was about 691 K (Hodak et al. 2000). They also found that the time scale of mixing at $T = 691$ K was at the range of seconds (Hodak et al. 2000). Because the self-diffusion coefficients of Ag and Au are identical, the interdiffusion coefficient of Au/Ag mixture can be taken to be the same as the self-diffusion coefficients (Hodak et al. 2000). Hence, using our previous model for the melting point of nanoparticles (Safaei et al. 2008), the value of T_{mp}/T_{mb} for the 20-nm-diameter Au nanoparticle is calculated as $T_{mp}/T_{mb} = 0.9584$. Here with the use of the values of $E_{ab} = 169.52$ kJ/mol and $DC_0 = 0.04$ cm²/s (Hodak et al. 2000) in Eq. 10, for the Au-core of 20 nm diameter, we have calculated the interdiffusion coefficient of Ag atoms into the Au-core at $T = 690$ K as $DC_{(20\text{nm}, 690\text{K})}^{\text{Ag} \rightarrow \text{Au}} = 2.0063 \times 10^{-14}$ cm²/s. Therefore, using $t = x^2/(6 \times DC)$, with x being the diffusion distance, i.e. $x = D/2 = 10$ nm (the Au-core radius), we have calculated the time scale for mixing Ag atoms into the Au-core as $t_{T=690\text{K}} = 8.311$ s which is well consistent with the experimentally obtained time scale (Hodak et al. 2000). Hodak et al. (2000) have also experimentally found that the interdiffusion coefficient of Ag atoms into the Au-core of $D = 20$ nm for absorbed energy of about 1.16 mJ/pulse (and therefore, for the sample temperature of $T = 1100$ K) was about $\approx 10^{-10}$ cm²/s, and the time scale needed for alloying of Au/Ag core–shell particles in this condition ($T = 1100$ K) was estimated to be in the range of microseconds. If we use the above parameters and $T = 1100$ K in Eq. 10 for the diameter of 20 nm, then we can find $DC_{(20\text{nm}, 1100\text{K})}^{\text{Ag} \rightarrow \text{Au}} = 7.70 \times 10^{-10}$ cm²/s and, therefore, $t_{T=1100\text{K}} = 216.37$ μ s, which are in agreement with the experimentally obtained values by Hodak et al. (2000) for the diffusion coefficient and the time scale of alloying at temperature 1100 K.

Based on this high value of the diffusion coefficient, i.e. $\approx 10^{-10}$ cm²/s, Hodak et al. (2000) concluded that their investigated particles were partially melted and the diffusion coefficients obtained by them were an average over the solid and the liquid portions of the nanoparticles. Therefore, they reported that the surface melting was the important phenomenon for the observed very fast, laser-induced interdiffusion/alloying of Au/Ag core–shell nanoparticles (Hodak et al. 2000). However, here, we suggest that the main mechanism for this faster-than-expected interdiffusion/alloying may not

be only the surface melting of the nanoparticles. Since the sample temperatures of 690 and 1100 K are well below the expected melting point of the 20-nm diameter Au-core [i.e. 1281.7 K estimated from our previous model (Safaei et al. 2008)] and also because our calculated values of the diffusion coefficients are for the *solid-phase particles* (nanocrystals), we can conclude that these interdiffusion coefficients are for the *solid-phase diffusion* and therefore Au/Ag alloying started and also, more importantly and interestingly enough, finished within the *solid phases*. Even if we assume that, at the experimental conditions of the reference (Hodak et al. 2000), the surface of the Au/Ag core–shell nanoparticles was melted, it is obvious that the Au-core of 20-nm diameter was not melted, and therefore, the Ag atoms diffused into the *solid-core* of Au. Assuming a liquid shell on the particle surface, one can conclude that the diffusion of Au atoms into the *melted* Ag-shell is much faster than the diffusion of Ag atoms into the *solid* Au-core. Hence, the timescale of this alloying, which is much faster than the usual bulk alloying, is equal to the timescale of its slower stage, i.e. the timescale needed for the Ag atoms to diffuse into the *solid* Au-core which is very slower than the diffusion of Au atoms into the *melted* Ag-shell. In other words, the rate of alloying of Au–Ag core–shell nanoparticles is dependent upon the rate of the diffusion of Ag atoms from the *melted* Ag-shell into the *solid* Au-core of the nanoparticles. Therefore, any mechanism describing this faster-than-expected alloying should focus on the diffusion of Ag atoms from the shell into the *solid* Au-core, namely should involve the *solid-phase diffusion* and not the surface melting phenomenon. Therefore, importantly, we suggest that this very fast alloying may be caused by some other reasons and not by the surface melting of the particles. According to Eq. 12, one can conclude that the size-dependent energetic and structural properties of nanoparticles directly influence their diffusion coefficients. Therefore, we may expect that the *reduced average coordination number* of nanoparticles and especially their *reduced surface coordination number* can give a possible explanation for this very fast interdiffusion/alloying. It is very important to notice that the volume structure and the binding energy of nanoparticles may be also size dependent, and therefore may have some effects on the diffusion process of Ag atoms into the *solid* Au-core. However, here, we have

neglected any possible size dependency of these volume properties of the nanoparticles.

Conclusion

We modeled the cohesive energy of nanocrystals in terms of the averaged structural and energetic features of their surface and volume. The simple direct proportion between the cohesive energy and the average coordination number of nanocrystals, derived in recent studies (Attarian Shandiz et al. 2008; Mirjalili and Vahdati-Khaki 2008; Attarian Shandiz 2008), has been obtained as a third-order approximation of the present model. We also demonstrated that such a simple proportion is an approximation that can be only applicable for a restricted number of elements, such as Al and Cu nanoparticles whose melting point reduction can be truly predicted by this simple proportion. Its consistency for Al and Cu nanoparticles implies the importance of the geometrical effects upon the cohesive energy. The failure of this simple direct proportion for some elements, particularly for Au nanoparticles, has been attributed to the size dependency of the ratio of ϵ_s/ϵ_v , which should be taken into account to correctly predict the size-dependent depression of cohesive energy of some elements. Also defining a new parameter, named as the surface-to-volume energy-contribution ratio, we have predicted the order of thermal stability of different surface faces of Cu nanoclusters in fully agreement with the MD results of the reference (Daff et al. 2009). Finally, we introduced a lattice-type-sensitive model for the size-dependent diffusion coefficient of atoms into nanocrystals, including the averaged structural and energetic features of the nanocrystals. We applied our model to the case of the mixing of Au_(core)–Ag_(shell) nanoparticles and found that our prediction is fully consistent with the experimentally obtained diffusion coefficient of Ag atoms into the Au core and with the experimental timescale of their interdiffusion/alloying. We interestingly suggest that any mechanism describing this faster-than-expected interdiffusion/alloying of Au_(core)–Ag_(shell) nanoparticles should take into account the *solid-phase diffusion* and not the surface melting phenomenon. According to our model, this faster-than-expected interdiffusion/alloying is due to some structural effects, such as the depression of the average coordination number of nanoparticles and

especially that of their surface. We think that a complete understanding of the mechanism of interdiffusion and alloying in nanoscaled crystals requires further investigation on their averaged structural and energetic features.

Appendix 1: Cohesive energy of nanocrystals

We assume that the total cohesion energy of each volume or surface atom of a nanocrystal is the sum of the contributions from both the first-nearest-neighbor (1NN) and the second-nearest-neighbor (2NN) atoms. Therefore, the total cohesive energy of a nanocrystal (E_{cn}) with n_t total atoms is:

$$E_{\text{cn}} = \sum_{i=1}^{n_v} \frac{1}{2} \left(Z_V^{(i)} \varepsilon_V^{(i)} + Z_V'^{(i)} \varepsilon_V'^{(i)} \right) + \sum_{i=1}^{n_s} \frac{1}{2} \left(Z_S^{(i)} \varepsilon_S^{(i)} + Z_S'^{(i)} \varepsilon_S'^{(i)} \right) \quad (14)$$

where n_v and n_s are the numbers of atoms located at the volume and the surface of the nanocrystal, respectively, and its total number of atoms is $n_t = n_v + n_s$. $Z_V^{(i)}$ and $Z_V'^{(i)}$ are the coordination numbers of volume atom i according to the 1NN and the 2NN definitions, respectively. $\varepsilon_V^{(i)}$ and $\varepsilon_V'^{(i)}$ are respectively the bond energies of volume atom i of the nanocrystal associated with the 1NN and 2NN atoms. Similar to the defined parameters of volume atoms, $Z_S^{(i)}$ and $Z_S'^{(i)}$ are the 1NN and 2NN coordination numbers of surface atom i of the nanocrystal, respectively. Note that Z_S is the number of the bonds of each surface atom without considering bonds to interior atoms. This definition of Z_S is due to its function in counting only the total number of the surface bonds of the crystal. Also, $\varepsilon_S^{(i)}$ and $\varepsilon_S'^{(i)}$ are the bond energies between surface atom i and its 1NN and 2NN atoms, respectively.

If we assume that the outer surface of the nanocrystal is composed of the number of N_f different crystalline faces, N_e different edges, and N_c corner sites on the surface, then we can rewrite Eq. 14 as follows:

$$E_{\text{cn}} = \sum_{i=1}^{n_v} \frac{1}{2} \left(Z_V^{(i)} \varepsilon_V^{(i)} + Z_V'^{(i)} \varepsilon_V'^{(i)} \right) + \sum_{j=1}^{N_f} \frac{1}{2} n_f^{(j)} \left(Z_f^{(j)} \varepsilon_f^{(j)} + Z_f'^{(j)} \varepsilon_f'^{(j)} \right) + \sum_{k=1}^{N_e} \frac{1}{2} n_e^{(k)} \left(Z_e^{(k)} \varepsilon_e^{(k)} + Z_e'^{(k)} \varepsilon_e'^{(k)} \right) + \sum_{m=1}^{N_c} \frac{1}{2} n_c^{(m)} \left(Z_c^{(m)} \varepsilon_c^{(m)} + Z_c'^{(m)} \varepsilon_c'^{(m)} \right) \quad (15)$$

where $n_f^{(j)}$ is the number of atoms located at each surface face j of the nanocrystal ($j = 1, 2, \dots, N_f$), $n_e^{(k)}$ is the number of atoms located at each surface edge k ($k = 1, 2, \dots, N_e$), and $n_c^{(m)}$ is the number of atoms located at each corner site m of the nanocrystal surface ($m = 1, 2, \dots, N_c$). The total number of atoms located at all the surface-crystalline faces is $n_f = \sum_{j=1}^{N_f} n_f^{(j)}$, the total number of atoms located at all the surface edges is $n_e = \sum_{k=1}^{N_e} n_e^{(k)}$, and that located at all the surface corners is $n_c = \sum_{m=1}^{N_c} n_c^{(m)}$. Therefore, the total number of the surface atoms of the nanocrystal is equal to $n_s = n_f + n_e + n_c$. Here, $Z_f^{(j)}$, $Z_f'^{(j)}$, $\varepsilon_f^{(j)}$, and $\varepsilon_f'^{(j)}$ are the previously defined parameters, but associated with the atoms located at surface-crystalline face j ; similarly, $Z_e^{(k)}$, $Z_e'^{(k)}$, $\varepsilon_e^{(k)}$ and $\varepsilon_e'^{(k)}$ are those parameters for the atoms located at surface edge k and $Z_c^{(m)}$, $Z_c'^{(m)}$, $\varepsilon_c^{(m)}$ and $\varepsilon_c'^{(m)}$ are for the atom of surface corner m . Here, we neglect any possible difference between the bond energies of atoms located at different surface faces, surface edges, and surface corners of the nanocrystal and assume that $\varepsilon_f^{(j)} = \varepsilon_e^{(k)} = \varepsilon_c^{(m)} = \varepsilon_s$, and $\varepsilon_f'^{(j)} = \varepsilon_e'^{(k)} = \varepsilon_c'^{(m)} = \varepsilon_s'$. Making this assumption also for all the volume atoms of the nanocrystal as $\varepsilon_V^{(i)} = \varepsilon_v$ and $\varepsilon_V'^{(i)} = \varepsilon_v'$, we can rewrite Eq. 15 as follows:

$$E_{\text{cn}} = \sum_{i=1}^{n_v} \frac{1}{2} \left(Z_V^{(i)} \varepsilon_v + Z_V'^{(i)} \varepsilon_v' \right) + \sum_{j=1}^{N_f} \frac{1}{2} n_f^{(j)} \left(Z_f^{(j)} \varepsilon_s + Z_f'^{(j)} \varepsilon_s' \right) + \sum_{k=1}^{N_e} \frac{1}{2} n_e^{(k)} \left(Z_e^{(k)} \varepsilon_s + Z_e'^{(k)} \varepsilon_s' \right) + \sum_{m=1}^{N_c} \frac{1}{2} n_c^{(m)} \left(Z_c^{(m)} \varepsilon_s + Z_c'^{(m)} \varepsilon_s' \right) \quad (16)$$

Denoting the 1NN-based average coordination number of atoms located at the surface faces as \bar{Z}_f , at the surface edges as \bar{Z}_e , and at the surface corners as \bar{Z}_c , we can write:

$$\bar{Z}_f = \frac{\sum_{j=1}^{N_f} n_f^{(j)} Z_f^{(j)}}{n_f}, \quad \bar{Z}_e = \frac{\sum_{k=1}^{N_e} n_e^{(k)} Z_e^{(k)}}{n_e}, \quad (17)$$

$$\bar{Z}_c = \frac{\sum_{m=1}^{N_c} n_c^{(m)} Z_c^{(m)}}{n_c}.$$

The 2NN-based definitions are also similar to Eq. 17 only with the corresponding notations, i.e. \bar{Z}_f' , \bar{Z}_e' , and \bar{Z}_c' . Using the above definitions, Eq. 16 can be rewritten as

$$E_{cn} = \sum_{i=1}^{n_V} \frac{1}{2} (Z_V^{(i)} \varepsilon_V + Z_V'^{(i)} \varepsilon_V') + \frac{1}{2} n_f (\bar{Z}_f \varepsilon_S + \bar{Z}_f' \varepsilon_S') + \frac{1}{2} n_e (\bar{Z}_e \varepsilon_S + \bar{Z}_e' \varepsilon_S') + \frac{1}{2} n_c (\bar{Z}_c \varepsilon_S + \bar{Z}_c' \varepsilon_S') \tag{18}$$

Here, we denote the average coordination numbers of the volume and surface atoms of the nanocrystal based on the 1NN (or 2NN) definition with \bar{Z}_V (or \bar{Z}_V') and \bar{Z}_S (or \bar{Z}_S'), respectively, and define them as follows:

$$\bar{Z}_V = \frac{\sum_{i=1}^{n_V} Z_V^{(i)}}{n_V}, \quad \bar{Z}_V' = \frac{\sum_{i=1}^{n_V} Z_V'^{(i)}}{n_V},$$

$$\bar{Z}_S = \frac{n_f \bar{Z}_f + n_e \bar{Z}_e + n_c \bar{Z}_c}{n_S}, \quad \bar{Z}_S' = \frac{n_f \bar{Z}_f' + n_e \bar{Z}_e' + n_c \bar{Z}_c'}{n_S},$$

$$n_S = n_f + n_e + n_c. \tag{19}$$

Using the above definitions, we can rewrite Eq. 18 as:

$$E_{cn} = \frac{1}{2} n_V (\bar{Z}_V \varepsilon_V + \bar{Z}_V' \varepsilon_V') + \frac{1}{2} n_S (\bar{Z}_S \varepsilon_S + \bar{Z}_S' \varepsilon_S') = n_V \bar{E}_V + n_S \bar{E}_S, \tag{20}$$

where $\bar{E}_V = (\bar{Z}_V \varepsilon_V + \bar{Z}_V' \varepsilon_V')/2$ and $\bar{E}_S = (\bar{Z}_S \varepsilon_S + \bar{Z}_S' \varepsilon_S')/2$ are the average contributions of each volume and surface atom of the nanocrystal to its total cohesive energy, respectively. From Eq. 20, the cohesive energy of the bulk crystal (E_{cb}) can be obtained as

$$E_{cb} = n_{Vb} \bar{E}_{Vb} + n_{Sb} \bar{E}_{Sb} \tag{21}$$

Here and hereafter in this article, the subscript b indicates the corresponding parameters for the bulk material, e.g., n_{Vb} and n_{Sb} are the numbers of atoms located at the volume and the surface of a bulk crystal, respectively, having the total number of n_t atoms. One may conclude that for a bulk crystal with n_t total atoms: $n_{Sb} \approx 0$ and $n_{Vb} \approx n_t$. Therefore, using Eqs. 20 and 21, we can write:

$$\frac{E_{cn}}{E_{cb}} = \frac{n_V \bar{E}_V + n_S \bar{E}_S}{n_{Vb} \bar{E}_{Vb} + n_{Sb} \bar{E}_{Sb}} = \frac{n_V \bar{E}_V + n_S \bar{E}_S}{n_t \bar{E}_{Vb}}$$

$$= \frac{\bar{E}_V}{\bar{E}_{Vb}} \left(1 - \left(1 - \frac{\bar{E}_S}{\bar{E}_V} \right) \frac{n_S}{n_t} \right), \tag{22}$$

$$\Gamma = \frac{\bar{E}_S}{\bar{E}_V}.$$

Appendix 2: Cohesive energy and average coordination number of nanocrystals

Considering the definitions of the volume and the surface average-coordination numbers, given in

Eq. 19, we can define the 1NN- and 2NN-average coordination numbers of nanocrystals, denoted by \bar{Z}_n and \bar{Z}'_n respectively, as follows:

$$\bar{Z}_n = \frac{n_V \bar{Z}_V + n_S \bar{Z}_S}{n_V + n_S} = \bar{Z}_V \left(1 - \left(1 - \frac{\bar{Z}_S}{\bar{Z}_V} \right) \frac{n_S}{n_t} \right)$$

$$\bar{Z}'_n = \frac{n_V \bar{Z}'_V + n_S \bar{Z}'_S}{n_V + n_S} = \bar{Z}'_V \left(1 - \left(1 - \frac{\bar{Z}'_S}{\bar{Z}'_V} \right) \frac{n_S}{n_t} \right). \tag{23}$$

Equation 23 defines the average coordination numbers of a nanocrystal and can be used for nanoparticles, nanowires, nanofilms, and any other shape of nanocrystals with the appropriate value of the surface-to-volume atomic ratio (n_S/n_t). In this equation, the effects of the surface face, surface edge, and surface corner atoms have been taken into account. Now using Eq. 23 for adequately large and close-to-bulk nanocrystals ($n_S/n_t \rightarrow 0$), we have

$$\bar{Z}_b = \lim_{n_S/n_t \rightarrow 0} \bar{Z}_n = \lim_{n_S/n_t \rightarrow 0} \bar{Z}_V = \bar{Z}_{Vb}, \text{ and}$$

$$\bar{Z}'_b = \lim_{n_S/n_t \rightarrow 0} \bar{Z}'_n = \lim_{n_S/n_t \rightarrow 0} \bar{Z}'_V = \bar{Z}'_{Vb}, \tag{24}$$

where $\bar{Z}_b = \lim_{n_S/n_t \rightarrow 0} \bar{Z}_n$ gives a well-formulated definition for the 1NN average coordination number of the bulk crystal, which includes the effects of both of its surface and volume atoms and is equal to its volume (lattice) average coordination number, i.e. $\bar{Z}_b = \bar{Z}_{Vb}$, e.g., for a BCC lattice $\bar{Z}_b = \bar{Z}_{Vb} = 8$. Similarly \bar{Z}'_b is the bulk average coordination number, based on the 2NN definition. From Eqs. 23 and 24, we have:

$$\frac{\bar{Z}_n}{\bar{Z}_b} = \frac{\bar{Z}_V}{\bar{Z}_{Vb}} \cdot \left(1 - \left(1 - \frac{\bar{Z}_S}{\bar{Z}_V} \right) \frac{n_S}{n_t} \right)$$

$$\frac{\bar{Z}'_n}{\bar{Z}'_b} = \frac{\bar{Z}'_V}{\bar{Z}'_{Vb}} \cdot \left(1 - \left(1 - \frac{\bar{Z}'_S}{\bar{Z}'_V} \right) \frac{n_S}{n_t} \right). \tag{25}$$

The above equations, which have similar form as Eq. 22, represent the 1NN/2NN-based average coordination number of nanocrystals in terms of their size.

Now using Eqs. 20 and 23 and with a little algebra, the cohesive energy of nanocrystals can be obtained in terms of the crystal average coordination numbers as follows:

$$E_{cn} = \frac{1}{2} n_t \varepsilon_V \bar{Z}_n \left(1 + \frac{\bar{Z}_S}{\bar{Z}_n} \left(\frac{\varepsilon_S}{\varepsilon_V} - 1 \right) \frac{n_S}{n_t} \right) + \frac{1}{2} n_t \varepsilon_V' \bar{Z}'_n \left(1 + \frac{\bar{Z}'_S}{\bar{Z}'_n} \left(\frac{\varepsilon'_S}{\varepsilon'_V} - 1 \right) \frac{n_S}{n_t} \right) \tag{26}$$

As it can be seen from Eq. 26, if we neglect the difference between the bond energies of the surface and volume atoms, i.e. assume $\varepsilon_v = \varepsilon_s = \varepsilon$ and $\varepsilon'_v = \varepsilon'_s = \varepsilon'$, then we can write: $E_{cn} = n_t \varepsilon \bar{Z}_n / 2 + n_t \varepsilon' \bar{Z}'_n / 2$ which can be easily obtained by counting the numbers of 1NN and 2NN atomic bonds and multiplying them by their corresponding bonding energies. Considering only 1NN atomic interactions, we can obtain $E_{cn} = n_t \varepsilon \bar{Z}_n / 2$ which is exactly the previously developed equation in the reference (Atarian Shandiz et al. 2008). Now, from Eq. 26, for the bulk crystal ($n_s/n_t \rightarrow 0$), we have:

$$\begin{aligned} E_{cb} &= \lim_{n_s/n_t \rightarrow 0} E_{cn} = \lim_{n_s/n_t \rightarrow 0} \left(\frac{1}{2} n_t \varepsilon_v \bar{Z}_n + \frac{1}{2} n_t \varepsilon'_v \bar{Z}'_n \right) \\ &= \frac{1}{2} n_t \varepsilon_{vb} \bar{Z}_b + \frac{1}{2} n_t \varepsilon'_{vb} \bar{Z}'_b \end{aligned} \quad (27)$$

Referring to Eq. 24, i.e. $\bar{Z}_b = \bar{Z}_{vb}$ and $\bar{Z}'_b = \bar{Z}'_{vb}$, it can be understood that Eq. (27) is similar to Eq. 21. Here, using Eqs. 26 and 27, leads to

$$\begin{aligned} \frac{E_{cn}}{E_{cb}} &= \frac{\varepsilon_v \bar{Z}_n}{\varepsilon_{vb} \bar{Z}_b + \varepsilon'_{vb} \bar{Z}'_b} \left(1 + \frac{\bar{Z}_s}{\bar{Z}_n} \left(\frac{\varepsilon_s}{\varepsilon_v} - 1 \right) \frac{n_s}{n_t} \right) \\ &+ \frac{\varepsilon'_v \bar{Z}'_n}{\varepsilon_{vb} \bar{Z}_b + \varepsilon'_{vb} \bar{Z}'_b} \left(1 + \frac{\bar{Z}'_s}{\bar{Z}'_n} \left(\frac{\varepsilon'_s}{\varepsilon'_v} - 1 \right) \frac{n_s}{n_t} \right) \end{aligned} \quad (28)$$

Appendix 3: Calculation of Γ for crystalline planes of FCC lattice

Here, we calculate the values of Γ for common crystalline faces of an FCC lattice, and in order to do this, we need the values of the 1-, 2-, and 3NN coordination numbers in each face.

The lattice unit cell of an FCC crystal is shown in Fig. 4. The position of each of the atoms in the lattice can be obtained with a vector, e.g., the position vector $\vec{A} = a(1/2, 0, 1/2)$ which represents the atom A, where a is the lattice constant of FCC. The atom O is located at the position $(0, 0, 0)$ of the Cartesian coordinates in which each position is defined by the position vector (x, y, z) . The distance between the atom A and all its nearest neighbors located at the corners of the cube and also at the centers of the lateral faces, e.g., $\vec{B} = a(0, 0, 1)$ and $\vec{C} = a(1, 1/2, 1/2)$, is equal to $|\vec{AB}| = |\vec{AC}| = a/\sqrt{2} = d$ (d is the atomic diameter). Therefore, atom A has $\bar{Z}_v = 12$ 1NN with the bond length of $L_{\text{bond}} = d$ and the bond energy of ε . The 2NN atoms of the atom A, are

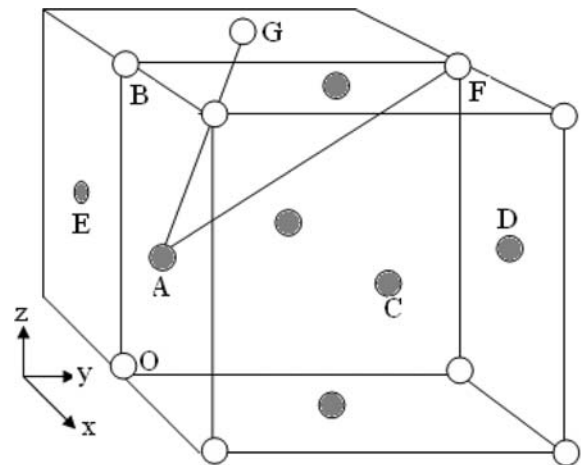


Fig. 4 A schematic illustration of the FCC lattice structure of Cu showing the first-order bonds ($L_{\text{bond}} = d$) between the 1NN atoms like as A–B and A–C, the second-order bonds ($L'_{\text{bond}} = d\sqrt{2}$) between the 2NN atoms like as A–E and A–D, and the third-order bonds ($L''_{\text{bond}} = d\sqrt{3}$) between the 3NN atoms like as A–F and A–G

atoms like E ($\vec{E} = a(-1/2, 0, 1/2)$) and D ($\vec{D} = a(1/2, 1, 1/2)$) located at the center of the adjacent and opposite faces of the A's face, respectively. Therefore, there are the number of $Z'_v = 6$ 2NN atoms for the atom A with the bond length of $L'_{\text{bond}} = a = d\sqrt{2}$ and the bond energy of ε' (note that $L'_{\text{bond}} = |\vec{AE}| = |\vec{AD}|$). As it can be seen from Fig. 4, the distance between atom F ($\vec{F} = a(0, 1, 1)$) and A is $|\vec{AF}| = |a(1/2, 0, 1/2) - a(0, 1, 1)| = a\sqrt{3}/2 = d\sqrt{3}$. There are eight atoms such as F in FCC lattice whose distances from atom A is $d\sqrt{3}$. One set of these atoms is $\{a(0, 1, 1), a(1, 1, 1), a(1, 1, 0), a(0, 1, 0)\}$ and the other set can be obtained by transferring this set of atoms through the vector $a(0, -2, 0)$, which is as follows: $\{a(0, -1, 1), a(1, -1, 1), a(1, -1, 0), a(0, -1, 0)\}$. Besides these sets of atoms, there are also another eight atoms, such as G, which are collected in the set $\{a(-1/2, 1/2, 1), a(-1/2, 1/2, 0), a(-1/2, -1/2, 0), a(-1/2, -1/2, 1)\}$, and the set $\{a(3/2, 1/2, 1), a(3/2, 1/2, 0), a(3/2, -1/2, 0), a(3/2, -1/2, 1)\}$ obtained by transferring the first set through the vector $a(2, 0, 0)$. The distance of all these atoms from atom A is equal to $d\sqrt{3}$ and, therefore, the 3NN atoms of atom A are the above mentioned 16 atoms ($Z''_v = 16$) with the bond length of $L''_{\text{bond}} = d\sqrt{3} = a\sqrt{3}/2$ and the bond

Table 1 The face and volume (lattice) coordination numbers (Z_f and Z_V) for different surface faces and lattice structures according to the 1-, 2-, and 3NN definitions

Lattice structure	Surface coordination numbers						Volume coordination numbers					
	1NN		2NN		3NN		1NN		2NN		3NN	
	nb	Z_f	nb'	Z'_f	nb''	Z''_f	Z_V	L_{bond}	Z'_V	L'_{bond}	Z''_V	L''_{bond}
SC												
(100)	1	4	4	4	–	0	6	$a = d$	12	$a\sqrt{2}$	0	–
(110)	2	2	5	4	–	0						
BCC												
(110)	2	4	2	2	5	2	8	$a\sqrt{3}/2 = d$	6	$a = 1.16 d$	12	$a\sqrt{2} = 1.63 d$
(100)	4	0	1	4	4	4						
(111)	4	0	3	0	3	6						
FCC												
(111)	3	6	3	0	4	6	12	$a\sqrt{2}/2 = d$	6	$a = d\sqrt{2}$	16	$a\sqrt{3}/2 = d\sqrt{3}$
(100)	4	4	1	4	16	0						
(110)	5	2	2	2	8	4						
(210)	6	0	2	2	8	4						

Also for each crystalline-face the number of its 1-, 2-, and 3NN broken bonds are shown which are respectively defined as $nb = (Z_V - Z_f)/2$, $nb' = (Z'_V - Z'_f)/2$ and $nb'' = (Z''_V - Z''_f)/2$. L_{bond} , L'_{bond} and L''_{bond} are the bond lengths between the 1-, 2-, and 3NN atoms, respectively. a and d are the lattice constant and the atomic diameter, respectively

energy of ϵ'' . The numbers of these 1-, 2-, and 3NN atoms for each atom located at the (111), (100), (110), and (210) faces of the FCC lattice can also be obtained in the same way and are collected in Table 1. Considering the definition of Γ , from Eq. 22, we can write the definition for each surface face (hkl) as follows:

$$\Gamma_{(hkl)} = \frac{Z_f^{(hkl)} \epsilon_f^{(hkl)} + Z'_f{}^{(hkl)} \epsilon'_f{}^{(hkl)} + Z''_f{}^{(hkl)} \epsilon''_f{}^{(hkl)}}{\bar{Z}_V \epsilon_V + \bar{Z}'_V \epsilon'_V + \bar{Z}''_V \epsilon''_V} \quad (29)$$

Now if we assume that the bond energies of atoms located in the volume and also at each type of surface faces are equal, i.e. $\epsilon_f^{(hkl)} = \epsilon_V = \epsilon$, $\epsilon'_f{}^{(hkl)} = \epsilon'_V = \epsilon'$ and $\epsilon''_f{}^{(hkl)} = \epsilon''_V = \epsilon''$, and if we use the values tabulated in Table 1, then we can calculate the factor $\Gamma_{(hkl)}$ for each of these faces as below:

$$\begin{aligned} \Gamma_{(111)} &= \frac{6\epsilon + 0 \times \epsilon' + 6\epsilon''}{12\epsilon + 6\epsilon' + 16\epsilon''}, & \Gamma_{(100)} &= \frac{4\epsilon + 4\epsilon' + 0 \times \epsilon''}{12\epsilon + 6\epsilon' + 16\epsilon''} \\ \Gamma_{(110)} &= \frac{2\epsilon + 2\epsilon' + 4\epsilon''}{12\epsilon + 6\epsilon' + 16\epsilon''}, & \text{and} & \\ \Gamma_{(210)} &= \frac{0 \times \epsilon + 2\epsilon' + 4\epsilon''}{12\epsilon + 6\epsilon' + 16\epsilon''} \end{aligned} \quad (30)$$

Since, in FCC lattice, the bond lengths of the 2NN and 3NN atoms are approximately equal, i.e. $L'_{\text{bond}} = d\sqrt{2} \cong L''_{\text{bond}} = d\sqrt{3}$, we can assume that their bond energies are also approximately identical, i.e. $\epsilon' \cong \epsilon''$. Therefore, we can finally write from Eq. 30

$$\begin{aligned} \Gamma_{(111)} &\cong \frac{6\epsilon + 6\epsilon'}{12\epsilon + 22\epsilon'}, & \Gamma_{(100)} &\cong \frac{4\epsilon + 4\epsilon'}{12\epsilon + 22\epsilon'}, \\ \Gamma_{(110)} &\cong \frac{2\epsilon + 6\epsilon'}{12\epsilon + 22\epsilon'}, & \text{and} & \Gamma_{(210)} \cong \frac{6\epsilon'}{12\epsilon + 22\epsilon'} \end{aligned} \quad (31)$$

References

Attarian Shandiz M (2008) Effective coordination number model for the size dependency of physical properties of nanocrystals. J Phys Condens Matter 20:325237–325245. doi:10.1088/0953-8984/20/32/325237

Attarian Shandiz M, Safaei A, Sanjabi S, Barber ZH (2008) Modeling the cohesive energy and melting point of nanoparticles by their average coordination number. Solid State Commun 145:432–437. doi:10.1016/j.ssc.2007.12.021

Buffat P, Borel J-P (1976) Size effect on the melting temperature of gold particles. Phys Rev A 13:2287–2298. doi: 10.1103/PhysRevA.13.2287

- Chacko S, Kanhere DG, Blundell SA (2005) First principles calculations of melting temperature for free Na clusters. *Phys Rev B* 71:155407–155412. doi:10.1103/PhysRevB.71.155407
- Daff TD, Saadouni I, Lisiecki I, de Leeuw NH (2009) Computer simulations of the effect of atomic structure and coordination on the stabilities and melting behaviour of copper surfaces and nano-particles. *Surf Sci* 603:445–454. doi:10.1016/j.susc.2008.11.031
- Delogu F (2005) Structural and energetic properties of unsupported Cu nanoparticles from room temperature to the melting point: molecular dynamics simulations. *Phys Rev B* 72:205418–205426. doi:10.1103/PhysRevB.72.205418
- DiCenzo SB, Berry SD, Hartford EH (1988) Photoelectron spectroscopy of single-size Au clusters collected on a substrate. *Phys Rev B* 38:8465–8468. doi:10.1103/PhysRevB.38.8465
- Dick K, Dhanasekaran T, Zhang Z, Meisel D (2002) Size-dependent melting of silica-encapsulated gold nanoparticles. *J Am Chem Soc* 124:2312–2317. doi:10.1021/ja017281a
- Hansen K-J (1960) Theoretische untersuchungen über den schmelzpunkt kleiner kugeln—ein beitrag zur thermodynamik der grenzflächen. *Z Phys* 157:523–553
- Hodak JH, Henglein A, Giersig M, Hartland GV (2000) Laser-induced inter-diffusion in AuAg core-shell nanoparticles. *J Phys Chem B* 104:11708–11718
- Jiang Q, Zhang Z, Wang YW (2000) Thermal stability of low dimensional crystals. *Mater Sci Eng A* 286:139–143. doi:10.1016/S0921-5093(00)00718-8
- Jiang Q, Zhang S, Zhao M (2003) Size-dependent melting point of noble metals. *Mater Chem Phys* 82:225–227. doi:10.1016/S0254-0584(03)00201-3
- Lai SL, Carlsson JRA, Allen LH (1998) Melting point depression of Al clusters generated during the early stages of film growth: nanocalorimetry measurements. *Appl Phys Lett* 72:1098–1100. doi:10.1063/1.120946
- Lide DR (ed) (2005) CRC Handbook of chemistry and physics. Internet Version 2005 <http://www.hbcpnetbase.com>. Thermal and physical properties of pure metals. CRC Press, Boca Raton, pp 12-219–12-220
- Lopez N, Janssens TVW, Clausen BS, Xu Y, Mavrikakis M, Bligaard T, Nørskov JK (2004) On the origin of the catalytic activity of gold nanoparticles for low-temperature CO oxidation. *J Catal* 223:232–235. doi:10.1016/j.jcat.2004.01.001
- Mansfield M, Needs RJ (1991) Surface energy and stress of lead (111) and (110) surfaces. *Phys Rev B* 43:8829–8833. doi:10.1103/PhysRevB.43.8829
- Mirjalili M, Vahdati-Khaki J (2008) Prediction of nanoparticles' size-dependent melting temperature using mean coordination number concept. *J Phys Chem Solids* 69:2116–2123. doi:10.1016/j.jpcs.2008.03.014
- Montejano-Carrizales JM, Aguilera-Granja F, Moran-Lopez JL (1997) Direct enumeration of the geometrical characteristics of clusters. *Nanostruct Mater* 8:269–287. doi:10.1016/S0965-9773(97)00168-2
- Nanda KK, Sahu SN, Behera SN (2002) Liquid-drop model for the size-dependent melting of low-dimensional systems. *Phys Rev A* 66:013208–013215. doi:10.1103/PhysRevA.66.013208
- Needs RJ, Mansfield M (1989) Calculations of the surface stress tensor and surface energy of the (111) surfaces of iridium, platinum and gold. *J Phys Condens Matter* 1:7555–7563. doi:10.1088/0953-8984/1/41/006
- Pawlow P (1909) Über die abhängigkeit des schmelzpunktes von der oberflächenenergie eines festen körpers. *Z Phys Chem* 65:545–548
- Rao CNR, Kulkarni GU, Thomas PJ, Edwards PP (2002) Size-dependent chemistry: properties of nanoparticles. *Chem Eur J* 8:28–35. doi:10.1002/1521-3765(20020104)8:1<28:AID-CHEM28>3.0.CO;2-B
- Safaei A, Attarian Shandiz M, Sanjabi S, Barber ZH (2007) Modelling the size effect on the melting temperature of nanoparticles, nanowires and nanofilms. *J Phys Condens Matter* 19:216216–216224. doi:10.1088/0953-8984/19/21/216216
- Safaei A, Attarian Shandiz M, Sanjabi S, Barber ZH (2008) Modeling the melting temperature of nanoparticles by an analytical approach. *J Phys Chem C* 112:99–105. doi:10.1021/jp0744681
- Salomons E, Griessen R, de Groot DG, Magerl A (1988) Surface tension and subsurface sites of metallic nanocrystals determined from H-absorption. *Europhys Lett* 5:449–454. doi:10.1088/0305-4608/16/12/009
- Solliard C, Flueli M (1985) Surface stress and size effect on the lattice parameter in small particles of gold and platinum. *Surf Sci* 156:487–494. doi:10.1016/0039-6028(85)90610-7
- Sun J, Simon SL (2007) The melting behavior of aluminum nanoparticles. *Thermochim Acta* 463:32–40. doi:10.1016/j.tca.2007.07.007
- Wang L, Zhang Y, Bian X, Chen Y (2003) Melting of Cu nanoclusters by molecular dynamics simulation. *Phys Lett A* 310:197–202. doi:10.1016/S0375-9601(03)00263-9
- Wautelet M (1998) On the shape dependence of the melting temperature of small particles. *Phys Lett A* 246:341–342. doi:10.1016/S0375-9601(98)00538-6
- Yang CC, Li S (2007) Investigation of cohesive energy effects on size-dependent physical and chemical properties of nanocrystals. *Phys Rev B* 75:165413–165417. doi:10.1103/PhysRevB.75.165413 (and references therein)